



Effect of PbS Thin Film Thickness with Cu-Doping on Thermoelectric Properties Using Spin Coating Method

R A Pahlevi, H Rahmadani, and M Diantoro*

Department of Physics, Faculty of Mathematics and Natural Science, Universitas Negeri Malang, Jl. Semarang 5, Malang, 65145, Indonesia.

*E-mail: markus.diantoro.fmipa@um.ac.id

Received
21 November 2021

Revised
07 April 2022

Accepted for Publication
20 July 2022

Published
09 October 2022



This work is licensed under a [Creative Commons Attribution-ShareAlike 4.0 International License](https://creativecommons.org/licenses/by-sa/4.0/)

Abstract

A thermoelectric device is produced from several materials that can convert heat into electrical energy or vice versa by generating the Seebeck effect and the Peltier effect. Then the energy can be formed from a heat source. This research used copper monosulfide (CuS) and lead monosulfide (PbS) as the primary materials for thermoelectric manufacture in the form of films. The method used in this research is a spin coating. This method uses the procedure of making a thin film on the substrate. The choice of this material is because CuS and PbS have high electrical conductivity and low thermal conductivity, so the value figure of merit (ZT) is high. From the thin film produced, an annealing process will be carried out to remove unwanted elements. After the sample is finished, the electrical conductivity test will be carried out with four probes, x-ray diffraction (XRD), and scanning electron microscopy (SEM). The four probes' conductivity test characterization results for one-layer, two-layers, and three-layers variations are 27.4 S/m, 53.6 S/m, and 106.8 S/m, respectively. From the SEM results, the grain size obtained from one-layer, two-layers, and three-layers variations are 227.9 nm, 397.8 nm, and 269.6 nm, respectively. Based on the XRD results, the crystal size obtained for variations of one-layer, two-layers, and three-layers has a size of 43.65 nm, 43.55 nm, and 43.60 nm, respectively. Furthermore, the lattice parameter has the same value from each sample variation, which is 5.93 Å.

Keywords: CuS, PbS, thin film, thermoelectric, spin coating.

1. Introduction

A thermoelectric device is a technology that can directly convert heat energy into electrical energy [1], [2]. In principle, this technology uses a material that can collect thermal energy and convert it into electrical energy [1]–[4]. This thermoelectric focuses on the temperature difference between objects with high and low temperatures [5], [6]. Collecting materials and converting heat into electrical energy can be necessary research to be developed in the future.

The thermoelectric efficiency of a system is described by the figure of merit (ZT) [6]–[8], where the figure of merit is influenced by the value of thermal conductivity, Seebeck coefficient, and electrical conductivity [6]–[10]. The good thermoelectric can be seen with a prominent figure of merit value, which indicates that the thermoelectric efficiency is good [11], [12]. Thermal and electrical conductivities are affected by the materials used in thermoelectric synthesis. Good electrical conductivity mostly comes from materials that are conductors [13].

Recently, thermoelectric effects on nanostructured materials and low-dimensional systems have attracted attention. Advances in nanoscale experimental techniques have been widely developed to form fabricated structures with higher thermoelectric efficiency than ordinary bulk materials [13]–[15]. That opens up a new perspective for developing more extensive thermoelectric energy conversion.

So far, thermoelectric thin films have been manufactured without adding other materials, but the results obtained do not provide an enormous electrical conductivity value [15]–[17]. In addition, the resulting thermal conductivity has an enormous value. That makes the thermoelectric have a small efficiency [15]–[19]. For this reason, it is necessary to do further research on thermoelectrics that can provide a prominent figure of merit value.

In this research, a thermoelectric lead monosulfide (PbS) thin film with copper (Cu) doped will be made and will vary its thickness which is expected to increase the value of the figure of merit [4]. Cu was chosen as doping because it is an element that has good conductor properties and a low melting point [20]. In addition, Cu is relatively cheap and easy to get.

2. Method

PbS nanoparticles were synthesized by mixing PbS in tetra ethylene glycol (TEG). Then the solution was stirred using a magnetic stirrer for two hours, and copper monosulfide (CuS) was added to the PbS. The solution given CuS has then stirred again with a magnetic stirrer for two hours at room temperature. The PbS solution added with CuS is then deposited on a glass substrate that has been sterilized using alcohol. Then spin coating on the substrate with a rotation speed of 2000 rpm for one minute. The sample was then heated at 100 °C for one hour.

Samples were characterized using x-ray diffraction (XRD) to determine the crystal size of the sample. Furthermore, the shape and morphology characterization using scanning electron microscopy (SEM). The electrical conductivity test was characterized using the I-V meter four-point probe to determine the effect of thickness on electrical conductivity.

3. Result and Discussion

3.1. XRD Characterization Results

The XRD was carried out using a diffraction pattern of 20–60° with a wavenumber of Cu-K α . To determine the value of crystal size and crystal structure, it is necessary to have the value of the diffraction peak and intensity [21], as is shown in Figure 1a. The diffraction peak at 2 θ (25.7°, 29.8°, 42.7°, 51.8°, and 54.2°) from the XRD results corresponds to the PbS crystallography open database (COD) number 9013403. The PbS crystal formed has a cubic crystal system, a space group of Fm-3m, and lattice parameters 5.93 Å. The resulting lattice parameters on the one-layer, two-layers, and three-layers samples are $a = b = c = 5.93$ Å. The lattice parameter has the same value for all layers because the variation used is the thickness, and there is no addition of materials other than Cu. The values for parameters a , b , and c are the same because the crystal structure is cubic, as shown in Figure 1b.

The crystal size of Cu-doped PbS can be obtained using the Scherrer equation (Equation 1),

$$D = \frac{k\lambda}{\beta \cos \theta} \quad (1)$$

where λ is the wavelength of Cu-K α , β is the full width at half maximum (FWHM), and θ is the Bragg angle or diffraction angle. The value of k is 0.9, which is obtained from the fitting results that depend on the shape of the crystal. The FWHM value is affected by the intensity of the crystal plane obtained from the highest peak, and the FWHM value must be in radians. The crystal size of the sample is shown in Table 1.

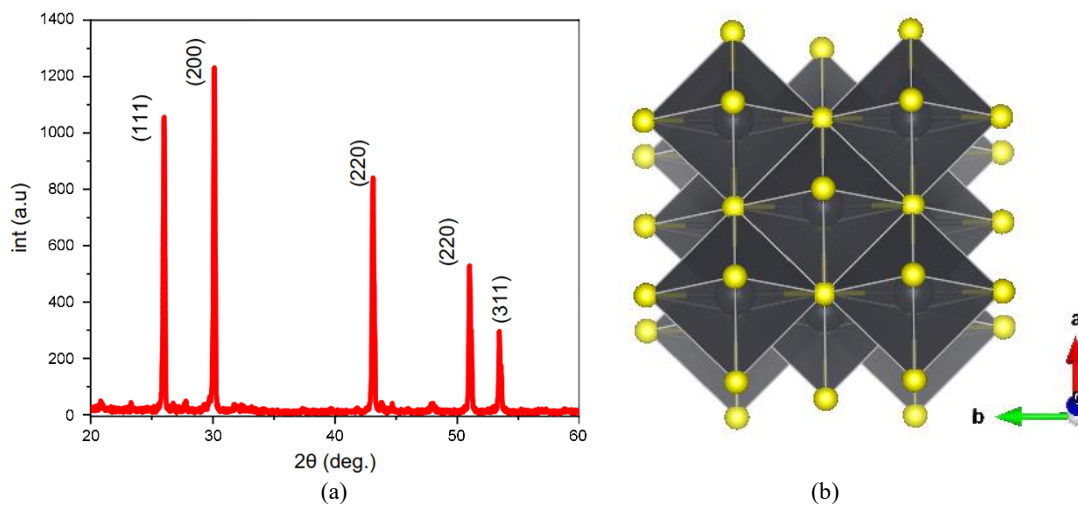


Figure 1. (a) XRD results of Cu-doped PbS and (b) PbS crystal structure with spin coating method.

Table 1. Crystal size of each sample by spin coating method.

Thickness	Crystal Size
One-layer	43,65 nm
Two-layers	43,55 nm
Three-layers	43,60 nm

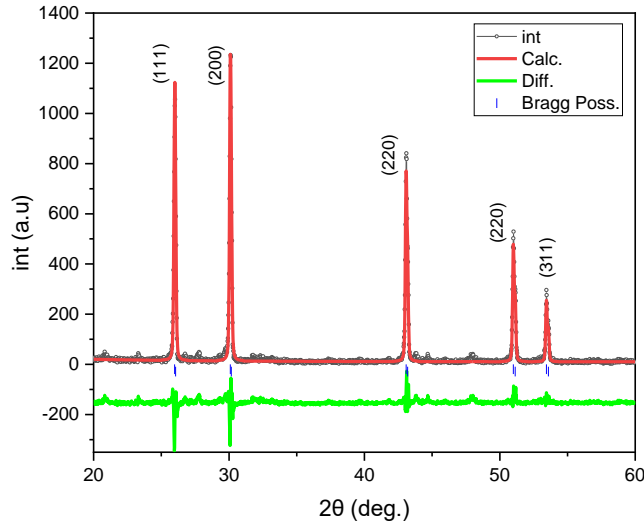


Figure 2. Gaussian fitting results from Cu-doped PbS XRD.

Figure 2 shows the results of fitting Rietveld refinement using Rietica with a goodness of fit (GOF) test of 2.61. The results are a cubic crystal system, space group Fm-3m, lattice parameter is 5.93 Å, and volume is 208.9 Å³.

3.2. SEM Characterization Results

SEM characterization was used to determine the morphology and distribution of particles in the sample. Figure 3 shows the Cu-doped PbS SEM with a glass substrate's spin coating method. It is known from the SEM results that the grain size and shape of the particles are spherical and oval. Grain size is influenced by several factors, i.e. the temperature at which the sample is annealed, the time of stirring the sample, and the type of material [13]. Figure 4 shows the results of the analysis of the Cu-doped PbS SEM using the spin coating method. Table 2 shows the grain size of each sample.

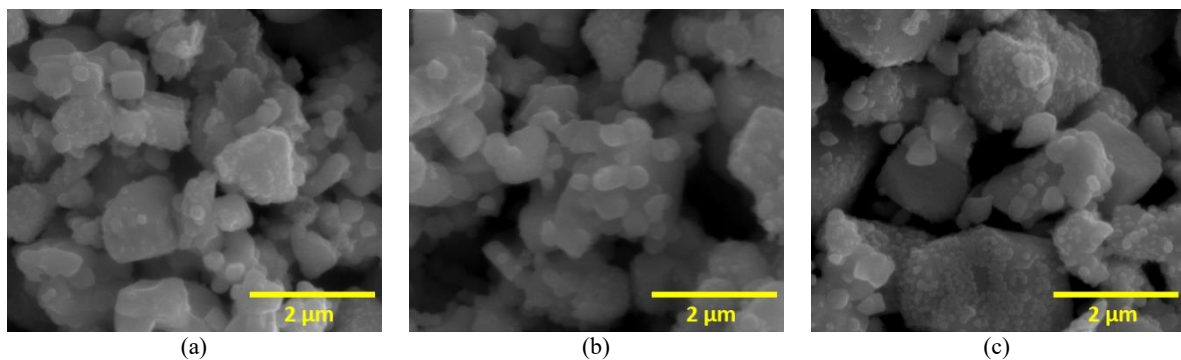


Figure 3. SEM results of Cu-doped PbS samples (a) one-layer, (b) two-layers, and (c) three-layers, with spin coating method.

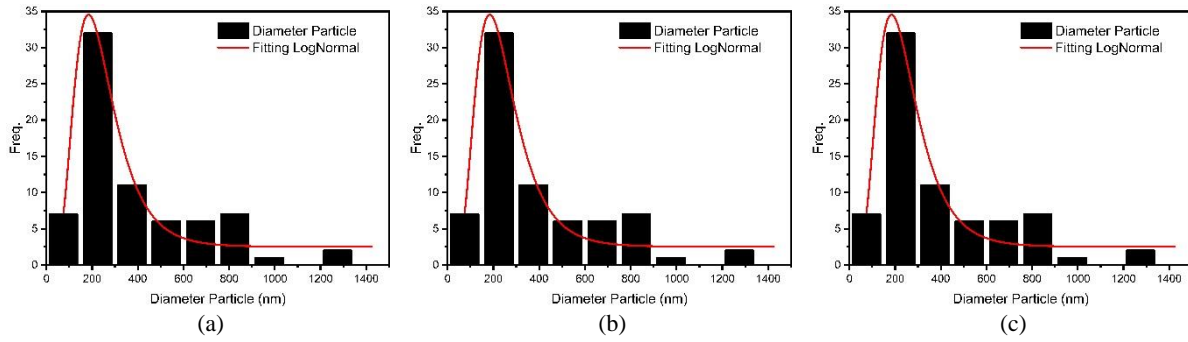


Figure 4. Results of the PbS distribution analysis of Cu-doped samples (a) one-layer, (b) two-layers, and (c) three-layers.

Table 2. Grain size of Cu-doped PbS with thickness variations.

Thickness	Grain Size
One-layer	227.9 nm
Two-layers	397.8 nm
Three-layers	269.6 nm

3.3. The I-V Meter Four Point Probe Characterization Results

The characterization of the I-V meter four-point probe aims to determine the value of the electrical conductivity of the sample. Characterization is done by comparing the thickness of the sample with the value of electrical conductivity [16]. The results obtained from the characterization of the I-V meter four-point probe are shown in Table 3. The results show that the conductivity value increases with thickness. The resulting conductivity is worth 10^2 and can categorize as a large conductivity. Figure 5 is a graph of the relationship between thickness and conductivity values.

Table 3. Electrical conductivity values with thickness variations.

Thickness	Electrical Conductivity
One-layer (0,124 mm)	27.4 S/m
Two-layers (0,139 mm)	53.6 S/m
Three-layers (0,241 mm)	106.8 S/m

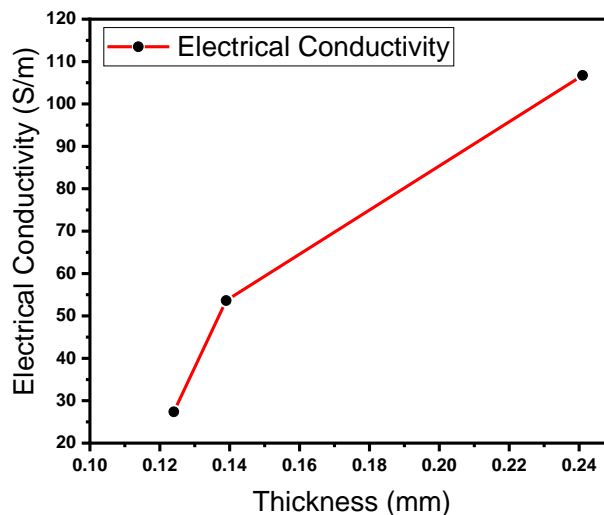


Figure 5. Graph of thickness relationship with electrical conductivity value.

4. Conclusion

The effect of thin layer thickness on thermoelectric Cu-doped PbS on crystal size is known that variations of one-layer, two-layers, and three-layers are 43.65 nm, 43.54 nm, and 43.60 nm, respectively. The lattice parameter of PbS thermoelectric with Cu doping has a value of $a = b = c = 5.93$ Å for each thickness variation has the same lattice parameter value. The grain size of each variation of one-layer, two-layers, and three-layers has a size of 227.9 nm, 397.8 nm, and 269.6 nm, respectively. Based on the results of SEM, PbS with Cu doping has a round and oval grain shape. At the same time, the thickness of the Cu-doped PbS layer has a directly proportional relationship with the electrical conductivity value. The electrical conductivity values for the variation of one-layer, two-layers, and three-layers in a row are 27.4 S/m, 53.6 S/m, and 106.8 S/m by multiplying 10^2 .

Acknowledgement

Our gratitude goes to the Universitas Negeri Malang, which has funded research through the Student Innovation (INOMA) scheme through the PNPB 2021 with a contract of 5.3.560/UN32.14.1/LT/2021.

References

- [1] H. Li *et al.*, “Enhanced thermoelectric performance of carbon nanotubes/polyaniline composites by multiple interface engineering,” *ACS Appl. Mater. Interfaces*, vol. 13, no. 5, pp. 6650–6658, 2021, doi: [10.1021/acsami.0c20931](https://doi.org/10.1021/acsami.0c20931).
- [2] F. H. Lin and C. J. Liu, “Energy-efficient synthesis and high thermoelectric performance of α - $\text{Cu}_{2-y}\text{Se}_{1-x}\text{Te}_x$,” *ChemSusChem.*, vol. 14, no. 5, pp. 1316–1323, 2021, doi: [10.1002/cssc.202002748](https://doi.org/10.1002/cssc.202002748).
- [3] Y. Luo *et al.*, “Cubic AgMnSbTe_3 semiconductor with a high thermoelectric performance,” *J. Am. Chem. Soc.*, vol. 143, no. 34, pp. 13990–13998, 2021, doi: [10.1021/jacs.1c07522](https://doi.org/10.1021/jacs.1c07522).
- [4] C. Chang and M. Ibáñez, “Enhanced thermoelectric performance by surface engineering in SnTe-PbS nanocomposites,” *Materials*, vol. 14, no. 18, p. 5416, 2021, doi: [10.3390/ma14185416](https://doi.org/10.3390/ma14185416).
- [5] D. S. Nkemeni, Z. Yang, S. Lou, G. Li, and S. Zhou, “Achievement of extra-high thermoelectric performance in doped copper (I) sulfide,” *J. Alloys Compd.*, vol. 878, p. 160128, 2021, doi: [10.1016/j.jallcom.2021.160128](https://doi.org/10.1016/j.jallcom.2021.160128).
- [6] Y. Liu *et al.*, “Defect engineering in solution-processed polycrystalline SnSe leads to high thermoelectric performance,” *ACS nano*, vol. 16, no. 1, pp. 78–88, 2021, doi: [10.1021/acsnano.1c06720](https://doi.org/10.1021/acsnano.1c06720).
- [7] J. Pei *et al.*, “Weak-ferromagnetism for room temperature thermoelectric performance enhancement in p-type $(\text{Bi,Sb})_2\text{Te}_3$,” *Mater. Today Phys.*, vol. 19, p. 100423, 2021, doi: [10.1016/j.mtphys.2021.100423](https://doi.org/10.1016/j.mtphys.2021.100423).
- [8] J. Wei *et al.*, “Enhanced thermoelectric performance of low carbon cement-based composites by reduced graphene oxide,” *Energy Build.*, vol. 250, p. 111279, 2021, doi: [10.1016/j.enbuild.2021.111279](https://doi.org/10.1016/j.enbuild.2021.111279).
- [9] S. Sarkar *et al.*, “Dissociation of GaSb in n-type PbTe : off-centered Gallium atom and weak electron–phonon coupling provide high thermoelectric performance,” *Chem. Mater.*, vol. 33, no. 5, pp. 1842–1851, 2021, doi: [10.1021/acs.chemmater.0c04854](https://doi.org/10.1021/acs.chemmater.0c04854).
- [10] T. Y. Su *et al.*, “Thermally strain-induced band gap opening on platinum diselenide-layered films: A promising two-dimensional material with excellent thermoelectric performance,” *Chem. Mater.*, vol. 33, no. 10, pp. 3490–3498, 2021, doi: [10.1021/acs.chemmater.0c04351](https://doi.org/10.1021/acs.chemmater.0c04351).
- [11] C. Tan *et al.*, “Enhanced thermoelectric performance of p-type sintered BiSbTe -based composites with AgSbTe_2 addition,” *Ceram. Int.*, vol. 47, no. 1, pp. 725–731, 2021, doi: [10.1016/j.ceramint.2020.08.182](https://doi.org/10.1016/j.ceramint.2020.08.182).
- [12] S. Yang *et al.*, “Ductile $\text{Ag}_{20}\text{S}_7\text{Te}_3$ with excellent shape-conformability and high thermoelectric performance,” *Adv. Mater.*, vol. 33, no. 10, p. 2007681, 2021, doi: [10.1002/adma.202007681](https://doi.org/10.1002/adma.202007681).
- [13] H. Zhang, H. Li, and F. Qu, “Synthesis of ZrNiSn with high thermoelectric performance via a novel high-gravity combustion method,” *Mater. Lett.*, vol. 293, p. 129745, 2021, doi: [10.1016/j.matlet.2021.129745](https://doi.org/10.1016/j.matlet.2021.129745).
- [14] P. Zhao *et al.*, “Thermoelectric performance of p-type $\text{Ca}_x\text{Fe}_{1.3}\text{Co}_{2.7}\text{Sb}_{12}$ skutterudites from high pressure synthesis,” *J. Alloys Compd.*, vol. 851, p. 156928, 2021, doi: [10.1016/j.jallcom.2020.156928](https://doi.org/10.1016/j.jallcom.2020.156928).

- [15] Z. Zheng *et al.*, “Rational band engineering and structural manipulations inducing high thermoelectric performance in n-type CoSb₃ thin films,” *Nano Energy*, vol. 81, p. 105683, 2021, doi: [10.1016/j.nanoen.2020.105683](https://doi.org/10.1016/j.nanoen.2020.105683).
- [16] D. Cadavid *et al.*, “Synthesis, bottom up assembly and thermoelectric properties of Sb-doped PbS nanocrystal building blocks,” *Materials*, vol. 14, no. 4, p. 853, 2021, doi: [10.3390/ma14040853](https://doi.org/10.3390/ma14040853).
- [17] T. Mao *et al.*, “Enhanced thermoelectric performance and service stability of Cu₂Se via tailoring chemical compositions at multiple atomic positions,” *Adv. Func. Mater.*, vol. 30, no. 6, p. 1908315, 2020, doi: [10.1002/adfm.201908315](https://doi.org/10.1002/adfm.201908315).
- [18] Q. Jiang *et al.*, “High Thermoelectric performance in n-type perylene bisimide induced by the solet effect,” *Adv. Mater.*, vol. 32, no. 45, p. 2002752, 2020, doi: [10.1002/adma.202002752](https://doi.org/10.1002/adma.202002752).
- [19] M. Safavi *et al.*, “Thermoelectric performance of Ge-doped Mg₂Si_{0.35}Sn_{0.65} thin films,” *J. Mater. Eng. Perform.*, vol. 30, no. 6, pp. 4045–4052, 2021, doi: [10.1007/s11665-021-05839-5](https://doi.org/10.1007/s11665-021-05839-5).
- [20] S. Battiston *et al.*, “One step synthesis and sintering of Ni and Zn substituted tetrahedrite as thermoelectric material,” *J. Alloys Compd.*, vol. 702, pp. 75–83, 2017, doi: [10.1016/j.jallcom.2017.01.187](https://doi.org/10.1016/j.jallcom.2017.01.187).
- [21] H. Liu *et al.*, “High-thermoelectric performance of TiO_{2-x} fabricated under high pressure at high temperatures,” *J. Materiomics*, vol. 3, no. 4, pp. 286–292, 2017, doi: [10.1016/j.jmat.2017.06.002](https://doi.org/10.1016/j.jmat.2017.06.002).
- [22] U. G. Jong, Y. S. Kim, C. H. Ri, Y. H. Kye, and C. J. Yu, “High thermoelectric performance in the cubic inorganic cesium iodide perovskites CsBI₃ (B = Pb, Sn, and Ge) from first-principles,” *J. Phys. Chem. C*, vol. 125, no. 11, pp. 6013–6019, 2021, doi: [10.1021/acs.jpcc.0c09929](https://doi.org/10.1021/acs.jpcc.0c09929).